analytical chemistry

Article

pubs.acs.org/ac

Chemical Imaging of Latent Fingerprints by Mass Spectrometry Based on Laser Activated Electron Tunneling

Xuemei Tang, Lulu Huang, Wenyang Zhang, and Hongying Zhong*

Key Laboratory of Pesticides and Chemical Biology, Ministry of Education, College of Chemistry, Central China Normal University, Wuhan, Hubei 430079, P. R. China

Supporting Information

ABSTRACT: Identification of endogenous and exogenous chemicals contained in latent fingerprints is important for forensic science in order to acquire evidence of criminal identities and contacts with specific chemicals. Mass spectrometry has emerged as a powerful technique for such applications without any derivatization or fluorescent tags. Among these techniques, MALDI (Matrix Assisted Laser Desorption Ionization) provides small beam size but has interferences with MALDI matrix materials, which cause ion suppressions as well as limited spatial resolution resulting from uneven distribution of MALDI matrix crystals with different sizes. LAET (Laser Activated Electron Tunneling) described in this work offers capabilities for chemical imaging through electron-directed soft ionization. A special film of semiconductors has been designed for collection of fingerprints. Nanoparticles of bismuth cobalt zinc oxide were compressed on a conductive metal substrate (Al or Cu sticky tape) under 10 MPa pressure. Resultant uniform thin films provide tight and shining surfaces on which fingers are impressed. Irradiation of ultraviolet laser pulses (355 nm) on the thin film instantly generates photoelectrons that can be captured by adsorbed organic molecules and subsequently cause electron-directed ionization and fragmentation. Imaging of latent fingerprints is achieved by visualization of the spatial distribution of these molecular ions and structural information-rich fragment ions. Atomic electron emission together with finely tuned laser beam size improve spatial resolution. With the LAET technique, imaging analysis not only can identify physical shapes but also reveal endogenous metabolites present in females and males, detect contacts with prohibited substances, and resolve overlapped latent fingerprints.

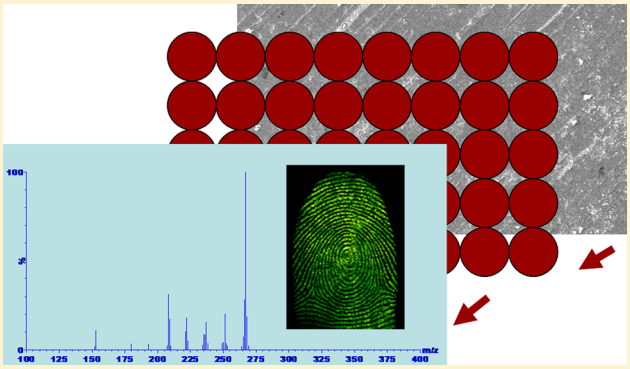

Although advanced genomics techniques such as DNA sequencing[1,2] have been more and more popular in criminal investigations, latent fingerprints (LFP) are still recognized as the useful form for identification of individuals and confirmation of identity because of the uniqueness and permanence of ridge patterns.[3,4] Characteristic fingerprint features are currently categorized as three levels[5] of which level 1 (pattern) and 2 (minutia) are mostly used. The level 1 feature is not unique but useful for macro classification including whorl, left loop, right loop, or arch classes. Level 2 features provide more detailed information such as ending, line fragment, and bifurcation. By using techniques with high resolution, level 3 features can be further established for sufficient discrimination of individuality based on all dimensional attributes of the ridge such as ridge path deviation, pores, edge contour, incipient ridges, breaks, creases, scars, or other permanent details.

In any case, level 1−level 3 features can only provide physical shape information. Recently developed techniques are more focused on molecular identification of exogenous and endogenous chemicals in a particular pattern which carry on more forensic information than just physical shapes.[6−8] It provides evidence for contacts of specific drugs,[9] prohibited substances,[10] or biomarkers from eccrine and sebaceous gland secretions.[11] For such purposes, many spectroscopic methods have been developed for enhanced LFP imaging such as fluorescence[12] and nanoplasmonic spectroscopy[13] as well as electrochemiluminescence.[14] However, these techniques often require chemical derivatization or addition of fluorescent tags. Fourier transform infrared[15] and Raman[16] do not need tags and have very good spatial resolution, but they cannot provide chemical information on latent fingerprints. In contrast, mass spectrometry-based imaging techniques can acquire numerous molecular information in a full scan manner with high sensitivity, selectivity, and accuracy but no sample preparation.[17−20] Among these techniques, DESI (Desorption Electro-Spray Ionization) offers distinguished capabilities for chemical imaging in a native environment.[21−24] The major difficulty associated with DESI is the spatial resolution that is limited by the intrinsic spray beam size. By controlling experimental conditions, the size of the most effective desorption/ionization

Received: October 3, 2014
Accepted: February 3, 2015
Published: February 3, 2015

DOI: 10.1021/ac504693v
Anal. Chem. 2015, 87, 2693−2701

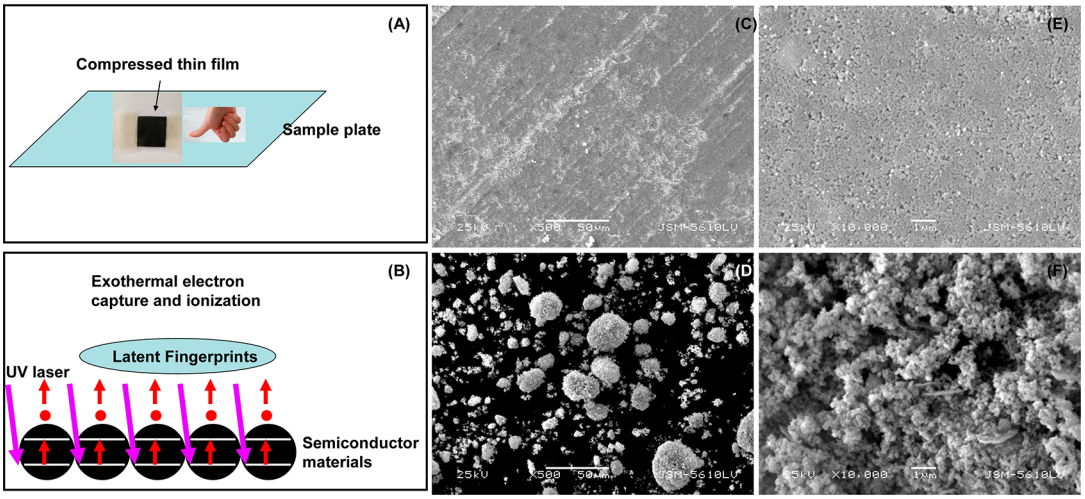

Figure 1. Collection of latent fingerprints on the surface of compressed thin film of $(Bi_2O_3)_{0.07}(CoO)_{0.03}(ZnO)_{0.9}$ (A), illustration of laser activated electron tunneling and capture (B) and surface comparisons between compressed (C, E) and noncompressed nanoparticles (D, F).

region of the spray impact plume can be decreased down to 40 μm.[25] Currently, MALDI (Matrix-Assisted Laser Desorption Ionization) provides spatial resolution that can be down to 5 μm, but it suffers from interferences with matrix materials.[26−28] Due to ion suppression in the low mass region and uneven distribution of crystal sizes, MALDI imaging has limited quantification ability.[29,30]

Unlike other mass spectrometry (MS) imaging methods, LAET (Laser Activated Electron Tunneling)[31] is an electron-directed soft ionization technique performed on the surface of semiconductor materials that have been compressed into a thin film under 10 MPa high pressure.[32] Upon laser irradiation, electrons in the valence bands are excited to conduction bands. Resultant photo generated electron−hole pairs are instantly separated and accelerated in the external static electric field. With appropriate kinetic energies, photoexcited electrons can escape away from the surface of semiconductors. Through the control of electric field, kinetic energies of photoexcited electrons are adjustable up to 100 eV that can cause further chemical bond cleavages. For example, at 20 eV energies, hot electrons are exothermally captured by charge-deficient atoms of adsorbed organic molecules, resulting in the formation of negatively charged odd-electron hypervalent molecular ions. Because the de Broglie wavelength of these electrons is less than regular organic bond length, the capture of these electrons does not cause redistribution of vibrational energies. Instead, it only initiates unpaired-electron directed specific α bond cleavages. Increased kinetic energies increase other nonspecific cleavages which complicate mass spectra. In this work, the detector is an electron multiplier. Resultant spatial resolution is determined by laser beam sizes, uniform distribution of semiconductor particles as well as areas from which the analytes ultimately are desorbed and ionized and other factors.

Major technical features of LAET mass spectrometry imaging are summarized as follows. (1) Compressed thin film of semiconductors offers uniform surface and uneven distribution of crystal sizes observed in regular MALDI is avoided. This feature enhances spatial resolution (the laser beam size is adjustable from 5 to 250 μm) and also makes it possible to achieve quantitative correlation between absolute intensities and sample quantities if there is no ion suppression interferences from sample matrix background. (2) Semiconductors do not generate peaks in the low mass region. Therefore, ion suppression effects of matrix materials are eliminated. (3) The kinetic energy of photoexcited electrons is controllable. It can be adjusted either by selection of different semiconductor nanoparticles that have different photocatalytic properties and electron mobility or by application of different bias voltages between the sample plate and the aperture. At 20 eV low energies, there are mainly negatively charged molecular ions and fragment ions resulting from the capture of tunneling electrons and subsequent unpaired electron-directed α bond cleavages, respectively. Compared with MS/MS experiments generated by the CAD (Collision Activated Dissociation) approach, mass spectra of LAET are easy to interpret because 20 eV energy does not cause nonspecific bond cleavages which are usually observed in regular CAD due to redistribution of vibrational energies. Additionally, in latent fingerprint imaging, because sampling is limited for each pixel, simultaneous generation of fragment ions without MS/MS experiments enhances confirmation of low abundance molecules and identification of unknowns. (4) Compared with other spectroscopic techniques, LAET MS imaging collects large amounts of molecular information in a full scan manner, but spectroscopic techniques establish imagings according to targeted molecular structures. (5) LAET is a clean ionization technique because semiconductor materials do not evaporate and ionize in the mass spectrometer. However, the LAET technique is still challenging for imaging analysis in native conditions which limits its applications to *in site* forensic investigation. It needs substrates on which fingers can be impressed. Second, unpaired electron-directed fragmentations complicate mass spectra although they may provide structural information for identification and validation of unknown molecules. In particular, LAET currently can only analyze small molecules because bigger molecules such as proteins or peptides are difficult to evaporate under such experimental conditions.

In this work, LAET was applied to latent fingerprint imaging by mass spectrometry including identification of physical shapes, detection of endogenous metabolites present in males and females, and deconvolution of overlapped fingerprints as well as investigation of contacts with drugs or other prohibited substances.

DOI: 10.1021/ac504693v
Anal. Chem. 2015, 87, 2693−2701

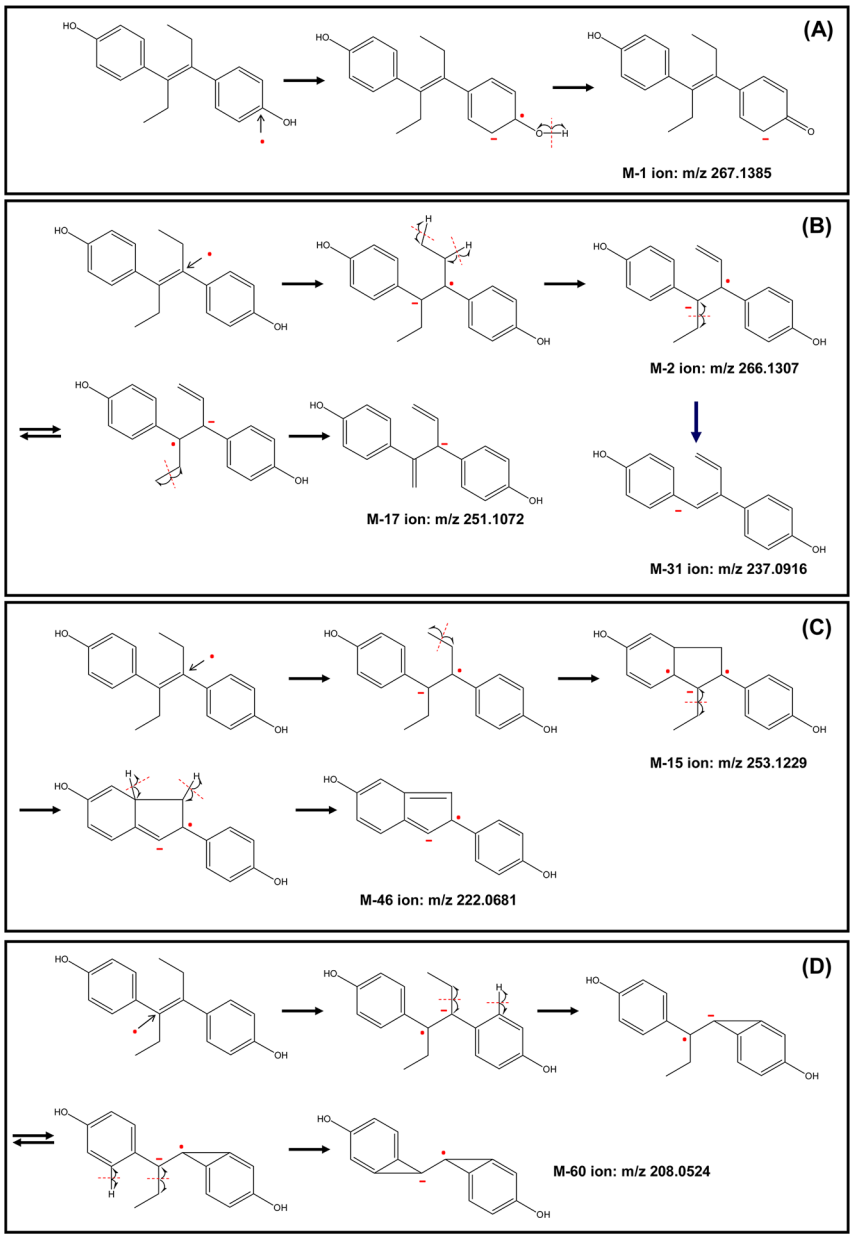

Figure 2. Capture of photogenerated electrons and unpaired-electron directed chemical bond cleavages of diethylstilbestrol.

EXPERIMENTAL SECTION

Reagents and Apparatus. LC-MS grade water was purchased from Fisher Scientific (NJ, USA). Nanoparticles of bismuth cobalt zinc oxide $(Bi_2O_3)_{0.07}(CoO)_{0.03}(ZnO)_{0.9}$ (<100 nm BET or <50 nm XRD), boron nitride, zinc oxide, gallium oxide, and aluminum nitride as well as dihydroxyl benzoic acid (DHB) were purchased from Sigma-Aldrich (MO, USA). All standard fatty acids (including C4:0, C6:0, C8:0, C10:0, C12:0, C14:0, C16:0, C18:0, C20:0 and C22:0) were purchased from Nu-ChekPrep Inc. (MN, USA). Diethylstilbestrol (DES) and dienestrol were purchased from Anpu (Shanghai, China). Ethanol was purchased from Guoyao (Tianjin, China). Nanoparticles have been thermally treated at 350 °C for 2 h in a muffle furnace (Hubei, China) before use in order to remove trace organic contaminants. Copper and alumina sticky tape was purchased from Junke (Shanghai, China).

Collection of Latent Fingerprints. Nanoparticles of bismuth cobalt zinc oxide $(Bi_2O_3)_{0.07}(CoO)_{0.03}(ZnO)_{0.9}$ were compressed on the sticky side of alumina or copper tape under 10 MPa high pressure with a compressor made by Keqi High and New Technology Co. (Tianjin, China). Other semiconductor materials can also be chosen so long as they have fast electron mobility and the UV laser energy of the mass spectrometer matches with their band gaps. As shown in Figure 1 (A), a shining and smooth thin film of semiconductor $(Bi_2O_3)_{0.07}(CoO)_{0.03}(ZnO)_{0.9}$ can be obtained. Fingerprints were collected on the surface of the thin film of $(Bi_2O_3)_{0.07}(CoO)_{0.03}(ZnO)_{0.9}$, and then the thin film was fixed on the MALDI sample plate. Figure 1 (B) shows the tunneling of photoexcited electrons and the capture by charge-deficient atoms of molecules present in latent fingerprints. Scan Electron microscope (JSM-5610LV, JEOL Ltd., Japan) has been used to compare surface properties of the thin film with that of noncompressed nanoparticles of $(Bi_2O_3)_{0.07}(CoO)_{0.03}(ZnO)_{0.9}$ as shown in Figure 1 (C) and (D), respectively. Figure 1 (E) and (F) are zoomed surfaces of

DOI: 10.1021/ac504693v
Anal. Chem. 2015, 87, 2693−2701

compressed thin film and noncompressed nanoparticles of $(Bi_2O_3)_{0.07}(CoO)_{0.03}(ZnO)_{0.9}$, respectively. Uneven distribution of nanoparticles has been observed in Figure 1 (D) and (F) because of aggregation. Instead, compression of these nanoparticles under high pressure provides a tight and relatively uniform surface for impression of fingers. Because nanoparticles of BN, AlN, ZnO, and Ga_2O_3 have distinguished photocatalytic properties, they have also been studied in this wok. Unfortunately, these materials cannot be compressed into such thin films and these particles usually stick to fingers.

Mass Spectrometric Imaging. The MALDI Synapt G2 HDMS system (Waters, USA) in negative mode was used for mass spectrometric imaging. It is equipped with an Nd:YAG high repetition laser head (355 nm). Spatial distribution of negatively charged molecular ions and fragment ions was obtained through scanning the laser beam across the sample plate. The step size has been set as 120 μm × 120 or 80 μm × 80 μm. Laser beam size is adjustable from 5 to 250 μm. In this work, the laser beam size was fixed at ≃15 μm. Laser influx has been set as 200 units. Laser pulse width is 3 ns, and laser fire rate was set as 1 Hz. Pulse energy is 100 μJ/200 Hz. For each pixel, the acquisition time is 1 s. Potential differences between the sample plate and the aperture were set as 20 V for all imaging experiments. Voltages on the sample plate and aperture are 87 and 107 V, respectively, for routine analysis. HDI software (Waters, US) was used for imaging analysis.

Assessment of the Quantitative Capability of the LAET Technique. The quantitative examination of the LAET technique was performed in solid state where 100 mg of $(Bi_2O_3)_{0.07}(CoO)_{0.03}(ZnO)_{0.9}$ nanoparticles have been mixed with 5 mg, 10 mg, 15 mg, 20 mg, and 25 mg of diethylstilbestrol (DES) solid particles, respectively. In each sample vial, 500 μL of ethanol solution was added. After these sample vials were extensively vortexed and diethylstilbestrol (DES) solid particles were dissolved, supernatant solutions in each vial were pipetted out, and nanoparticles were air-dried. Each 10 mg of these nanoparticles was compressed into a thin film for 5 repeated LAET experiments. The laser beam scans across the surface along a preset spiral route and the sampling time is 30 s for each experiment.

Calibration of Masses Measured by the MALDI Mass Spectromter in Negative Mode. Because small organic molecules are used as matrix materials in a regular MALDI technique, these small molecules produce extensive background peaks in the low mass range. Currently, there are no standard reagent kits commercially available for automatic mass calibration in the low mass range, especially in negative mode. In this work, the LAET technique does not produce interference peaks in the low mass range in negative mode. A standard solution of fatty acids containing C4:0, C6:0, C8:0, C10:0, C12:0, C14:0, C16:0, C18:0, C20:0, and C22:0 was made as a new calibration reagent kit. With UV (355 nm) laser irradiation, this standard solution spotted on surfaces of different semiconductor materials produces a series of uniform peaks ranging from 87.0446 to 339.3263 Da with about 28 Da mass differences between two adjacent peaks. The calibration was manually performed by using this standard solution as lock masses.

RESULTS AND DISCUSSION

Ionization and Fragmentation of Small Molecules on Surfaces of Different Semiconductor Materials Based on the LAET Mechanism. The key of LAET MS imaging technique is the photogeneration of hot electrons that can be accelerated and captured by charge deficient atoms of adsorbed organic molecules. Band gaps and electron mobility of semiconductor materials as well as external electric field determine electron tunneling possibilities and the final yield of electrons. By using a standard solution of diethylstilbestrol (100 μg/μL in ethanol) for proof-of-principle demonstration, we have investigated ionization and fragmentation mechanisms of this hormone on different semiconductor materials with ultraviolet laser irradiation (355 nm). Figure 2 (A) shows the structure of diethylstilbestrol (DES) and the production of a negative molecular ion at m/z 267.1385. Capture of photogenerated hot electrons by the carbon atom of the double bond adjacent to an −OH group not only switches neutral molecules to charged species but also generates odd-electron hypervalent species. The resultant unpaired electron further initiates α bond cleavage and generates a M-1 negative ion at m/z 267.1385. Photogenerated electrons can also be captured by other double bonds not present in the aromatic rings. A series of negative ions are theoretically expected as shown in Figure 2 (B-D) through unpaired-electron directed bond cleavages including m/z 266.1307, 251.1072, 237.0916, 222.0681, and 208.0524.

To validate the presence of these negative ions, diethylstilbestrol (DES) was deposited on the surfaces of different semiconductors to experimentally determine the molecular ion and fragment ions. The mass spectrometer was first calibrated with a standard solution of fatty acids containing C4:0, C6:0, C8:0, C10:0, C12:0, C14:0, C16:0, C18:0, C20:0, and C22:0. These fatty acids have been dissolved in acetone and deposited on the surfaces of $(Bi_2O_3)_{0.07}(CoO)_{0.03}(ZnO)_{0.9}$. Figure 3 (A) is the MS spectrum of this fatty acid mixture. It is shown that uniform peaks with 28 Da mass differences have been produced without background interferences.[31] This calibration ensures high mass accuracy in the low mass range for MALDI MS analysis of negative ions in high resolution mode. Figure 3 (B) is the MS spectrum of diethylstilbestrol (DES) deposited on the surfaces of BN. A dominant peak at m/z 267.1383 (error: 0.0002 Da) was observed, which represents the presence of M-1 negative ion. AlN generates similar spectrum as that of BN (data not shown). However, significantly different MS spectra have been obtained for diethylstilbesterol (DES) deposited on the surface of $(Bi_2O_3)_{0.07}(CoO)_{0.03}(ZnO)_{0.9}$ as shown in Figure 3 (C). In addition to the molecular ion at m/z 267.1389 (error: 0.0004 Da), several fragment ions have also been detected including ions at m/z 266.1326 (error: 0.0019 Da), 251.1067 (error: 0.0005 Da), 237.0918 (error: 0.0002 Da), 222.0671 (error: 0.0010 Da), and 208.0537 (error: 0.0013 Da). Table 1 summarizes all fragment ions observed with LAET techniques. Similar results have been obtained for ZnO and Ga_2O_3 materials (data not shown). In order to confirm that these fragment ions are truly produced from the molecular ion at m/z 267.1385, this ion has been isolated for tandem MS/MS experiments, and resultant MS/MS spectrum is shown in Figure 3 (D). Except for the ion at m/z 208.0537, the other ions have been observed. It should be indicated that all of these experiments have been performed with 20 V bias voltage between the sample plate and the aperture. When the bias voltage was increased to 70 V, BN also generates the same fragment ions shown as the inset of Figure 3 (C). These results have demonstrated that laser activated electron tunneling (LAET) indeed occurs in a MALDI Q-TOF mass spectrometer. Tunneling probability is affected by properties of semiconductors as well as the bias voltage between the sample

DOI: 10.1021/ac504693v
Anal. Chem. 2015, 87, 2693−2701

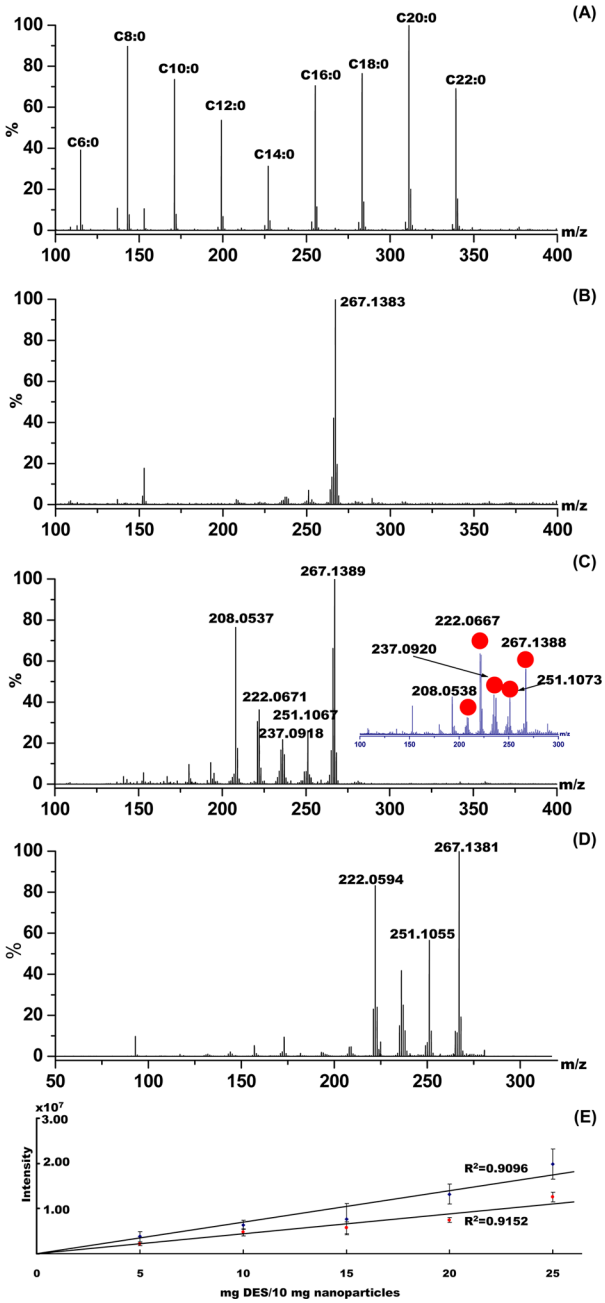

Figure 3. Production, fragmentation, and quantification of diethylstilbestrol based on the LAET MS technique with 20 V bias voltage between the sample plate and the aperture. (A) MS calibration with a standard solution containing C4-C22 free fatty acids. (B) MS spectrum of diethylstilbestrol spotted on BN. (C) MS spectrum of diethylstilbestrol spotted on $(Bi_2O_3)_{0.07}(CoO)_{0.03}(ZnO)_{0.9}$. Inset is the MS spectrum of diethylstilbestrol spotted on BN, but the bias voltage was 70 V. (D) MS/MS spectrum of the molecular ion of diethylstilbestrol spotted on BN. (E) Quantitative correlation between absolute mass spectrometric intensities and sample quantities for the molecular ion and a fragment ion.

plate and the aperture. When kinetic energies of electrons are high enough to escape away from the surfaces of semiconductors, they can be accelerated in the external electric field, captured by adsorbed organic molecules, and eventually initiate chemical bond cleavages. Although simultaneous production of fragment ions complicates mass spectra, it provides structure-rich information for validation of unknown molecules without

Table 1. Ionization and Fragmentation of Diethylstilbestrol Based on LAET

fragment ions	molecular formula	expt (Da)	obsd (Da)	error (Da)
M-1	$C_{18}H_{19}O_2$	267.1385	267.1389	0.0004
M-2	$C_{18}H_{18}O_2$	266.1307	266.1326	0.0019
M-17	$C_{17}H_{15}O_2$	251.1072	251.1067	0.0005
M-31	$C_{16}H_{13}O_2$	237.0916	237.0918	0.0002
M-46	$C_{15}H_{10}O_2$	222.0681	222.0671	0.0010
M-60	$C_{14}H_8O_2$	208.0524	208.0537	0.0013

MS/MS experiments. In the case of fingerprint analysis, the sampling for each pixel is very limited. Under such a situation, this feature enhances the capability of LAET to identify low abundance endogenous metabolites and exogenous chemicals.

Although deprotonation and subsequent negative charge-directed fragmentation in gas phase have been widely accepted in the past for interpretation of negatively charged ions detected by mass spectrometers, ions predicted in Figure 2 and observed in Figure 3 cannot be explained by the deprotonation mechanism. The major difference between ions generated by electron capture and deprotonation is that electron capture produces ions with unpaired electrons. These unpaired electrons are highly active to initiate α bond cleavages, while negative charges tend to break down adjacent bonds. In this work, electron capture and production of fragment ions from α bond cleavages have been confirmed with highly accurate masses. Additionally, it was demonstrated that different semiconductors generate different ions, indicating photocatalytic properties of solid surfaces of semiconductor nanoparticles play important roles in the ionization and fragmentation of organic molecules adsorbed on the surfaces instead of gas phase ion reactions.

Correlation of Absolute Mass Spectrometric Intensities and Sample Amounts. Because semiconductor materials do not generate background peaks, there is no ion suppression effect when a pure chemical is analyzed. In particular, nanoparticles have been compressed into a uniform thin film, quantitative correlation between absolute mass spectrometric intensities and sample amounts should be significantly improved because uneven distribution of matrix crystals with different sizes is decreased. In order to demonstrate the quantitative ability of the LAET technique, different amounts of solid diethylstilbestrol (DES) have been mixed with $(Bi_2O_3)_{0.07}(CoO)_{0.03}(ZnO)_{0.9}$ nanoparticles. In this work, we did not spot the diethylstilbestrol solution on the surface for quantitative demonstration because the solution may spread across the whole area. Figure 3 (E) shows correlative curves between absolute mass spectrometric intensities and sample quantities for the molecular ion (M-1) and a fragment ion (M-60). It was found all R values are more than 0.9. The same amounts of samples have also been mixed with a DHB solution that is a routinely used matrix material for regular MALDI analysis. Then it can be observed that mass spectrometric intensities dramatically fluctuate from one spot to another spot due to different sizes and distributions of DHB crystals as well as ion suppressions from DHB molecules. These experimental results confirm that the LAET technique can provide improved quantitative capability without interferences from background ions and matrix crystals.

However, while improved quantitative capability of LAET facilitates imaging analysis, effects of coexisted molecules (also

DOI: 10.1021/ac504693v
Anal. Chem. 2015, 87, 2693−2701

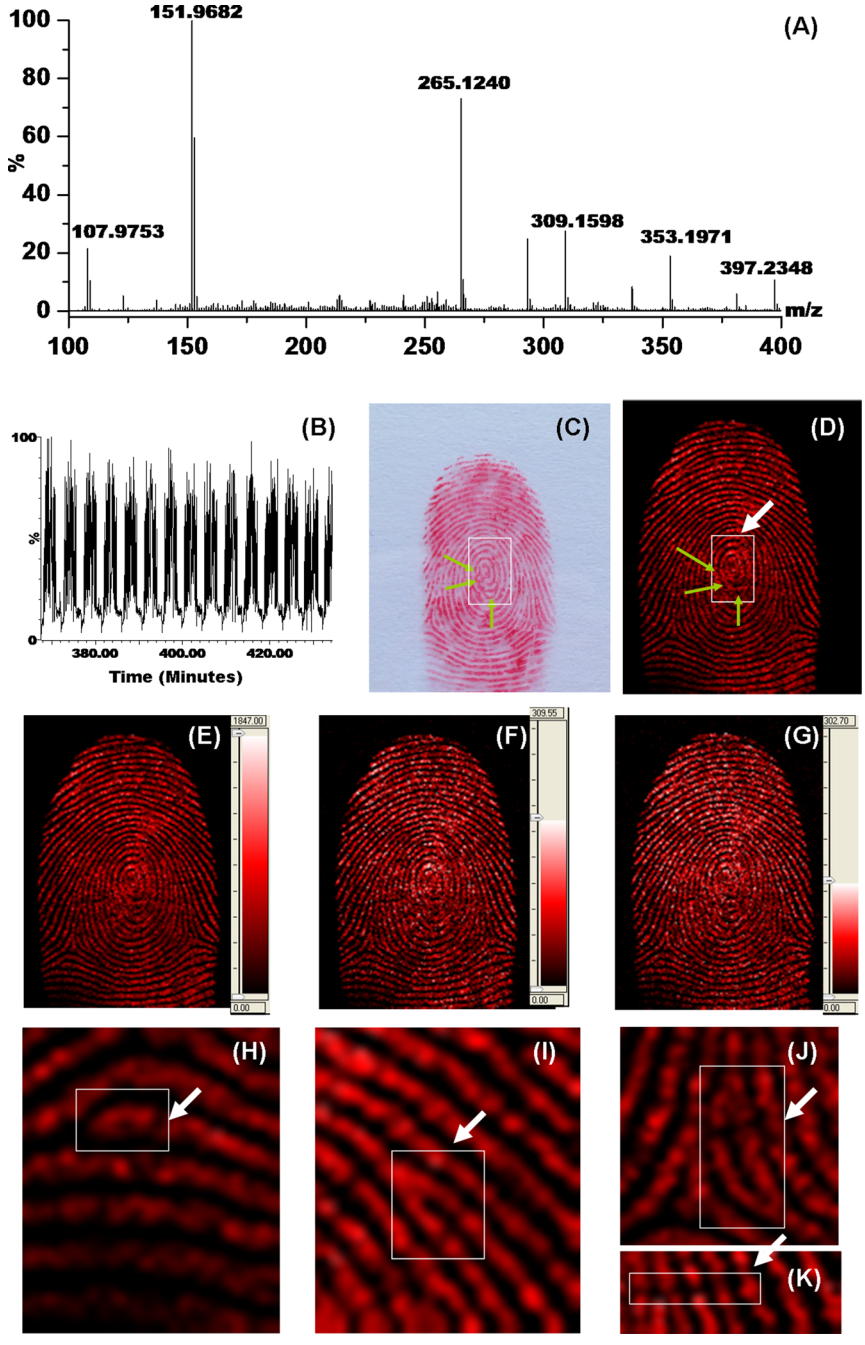

Figure 4. (A) Averaged MS spectrum of the latent fingerprint. (B) Total Ion Current (TIC) chromatogram of a latent fingerprint acquired with LAET MS imaging approach. (C) Red ink fingerprint blotted on a glass plate and optically photographed. Level 1 feature was shown as a whorl. (D) LAET MS imaging of this latent fingerprint with the same characteristics as that shown in optical imaging. (E) LAET MS imaging of this fingerprint at m/z 337 for a long chain fatty acid C22:1 as well as isotopic ions X+1 (F) and X+2 (G). Level 2 features including ending, bifurcation, and eye were shown in (H), (I), and (J), respectively. (K) shows a break that represents a level 3 feature.

called sample matrix) become the major challenge that still limits the quantification in MS imaging.

Imaging of Physical Shapes of Latent Fingerprints by the LAET MS Approach. When laser beam size is fixed at ~15 μm, step size of scanning as well as actual areas from which analytes are desorbed and ionizated becomes important factors in determining the quality of imaging. The laser beam size should be relatively smaller than that of step size. Bigger laser beam size may smear images because nearby analytes may be heated and ionized. At a step size of 120 μm × 120 μm, some minutia features or macro shapes are lost as shown in Supplementary Figure 1. Smaller step size results in higher imaging quality, but it takes a much longer time to complete data acquisition for the whole fingerprint. Taken together imaging quality and throughput, the step size was set at 80 μm × 80 μm in this section for proof of principle demonstration. Figure 4 (A) and (B) show a full scan MS spectrum of a clean female fingerprint and part of the total ion current (TIC) chromatogram, respectively. It can be found that total intensities of detected ions for each pixel are stable within the whole scanning area. In comparison with the optical imaging (with red ink) shown in Figure 4 (C), Figure 4 (D) is

DOI: 10.1021/ac504693v
Anal. Chem. 2015, 87, 2693−2701

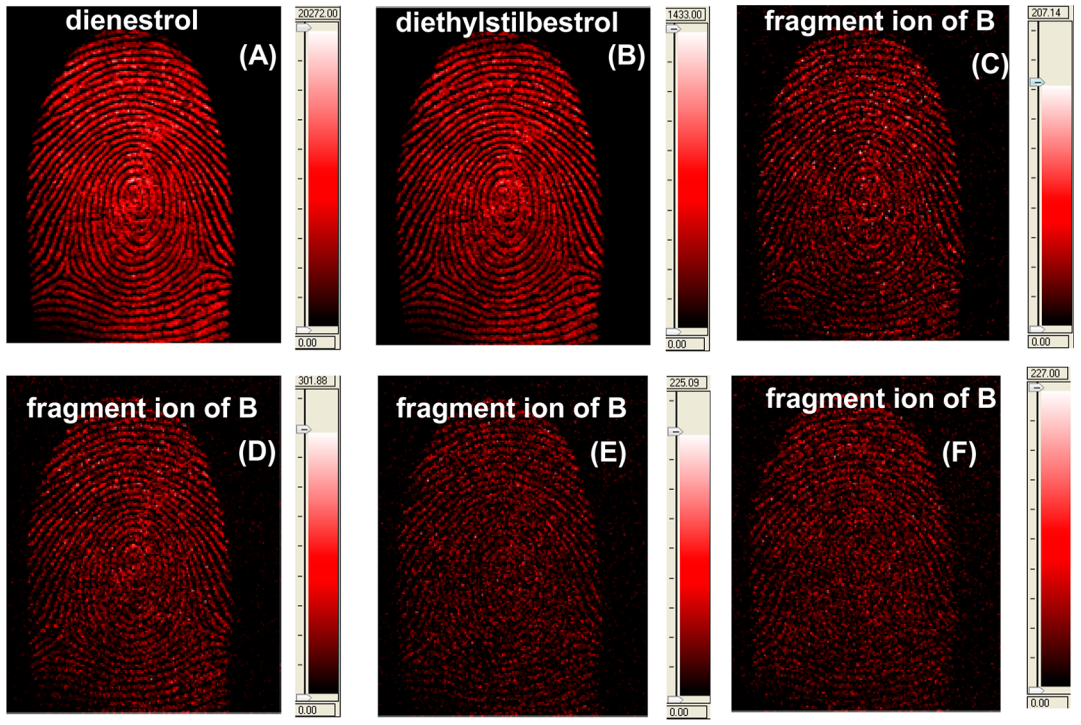

Figure 5. LAET MS imaging of a latent fingerprint at m/z 265.1240 for sex hormones dienestrol (A) and at m/z 267.1385 for diethylstilbestrol (B) as well as fragment ions expected at m/z 251.1072, 237.0916, 222.0681, and 208.0524 simultaneously generated from diethylstilbestrol (C–F).

the LAET MS chemical imaging of the same latent fingerprint. A whorl shape belongs to the level 1 feature with the same characteristics as that of optical imaging is shown in this figure. It is in the center of the fingerprint and also contains 3 eyes indicated as arrows. Figure 4 (E) shows the imaging at m/z 337.3012 (X) which represents a long chain fatty acid C22:1 from this sebum-rich latent fingerprint. Imagings of isotopic peaks including X+1 and X+2 were shown as Figure 4 (F) and (G). In general, LAET MS chemical imaging clearly shows all physical shapes contained in all level features. The presence of additional isotope peaks and the relative intensity ratio between X and X+1 confirms the identity of C22:1. Although the intensity of X+2 is higher than that of expected due to the overlap with another unknown molecule, clear images are still obtained, indicating LAET MS is capable of tolerating interferences. However, careful examination of these three images reveals that decreased signal intensities blur detailed structures because of background interferences. Figure 4 (H)-(K) are zoomed images cut from Figure 4 (E). Other level 2 features including ending and bifurcation as well as eye are shown in Figure 4 (H), (I), and (J), respectively. Figure 4 (K) shows a break in the fingerprint which provides level 3 information. All these characteristics describe the physical shape that is useful for fingerprint classification. With the MS approach, any ions included in the range of full scan can establish such images.

Revealing Endogenous Metabolites Present in Latent Fingerprints of Males and Females by the LAET MS Approach. Differentiation of male fingerprints and female fingers depends on substances from endogenous eccrine excretion of pheromones or metabolites and distinguished exogenous chemicals such as facial creams. Because eccrine sweat glands that are present in fingers do not extend deeply into the dermis, they excrete directly into the surface of the skin. Two typical estrogens dienestrol (expected at m/z 265.1229) and diethylstilbestrol (expected at m/z 267.1385) detected in female fingerprints are shown in Figure 5 (A) and (B), respectively. Male fingerprints may also contain these substances, but the intensities are comparatively very low as shown in Supplementary Figure 2. In addition to the molecular ion, fragment ions were generated without CAD MS/MS experiment as shown in Figure 2. Unpaired electron-directed α bond cleavage results in the formation of these ions. Figure 5 (C–F) show the images of fragment ions theoretically expected at m/z 251.1072, 237.0916, 222.0681, and 208.0524, respectively. Simultaneous formation of fragment ions together with molecular ions provides experimental evidence for enhanced identification of unknown molecules. This feature is especially important for latent fingerprint imaging. Additional tandem MS/MS experiments after full scans needs more sampling, but the total amount of analytes is extremely limited for each pixel.

In male fingerprints, androstadienone expected at m/z 269.1905 that is a metabolite of the sex hormone testosterone was also detected as shown in Supplementary Figure 3. Although none of level 1, level 2, and level 3 features was obtained due to very low intensity, the presence of this endogenous metabolite provides useful molecular clues for identity of individuals. Actually, there are tremendous other ions with enough intensity (such as previously described ions at m/z 337, 265, 267) in a full scan mass spectrometric experiment to establish the physical shape of latent fingerprints. Therefore, these low abundance ions complement with other ions for more detailed characterization of individual information. It should be indicated that levels of endogenous metabolites or exogenous chemicals vary with physiological status, diet, and ages. Differentiation of females and males based on levels of hormones present in latent fingerprints is not reliable.

DOI: 10.1021/ac504693v
Anal. Chem. 2015, 87, 2693–2701

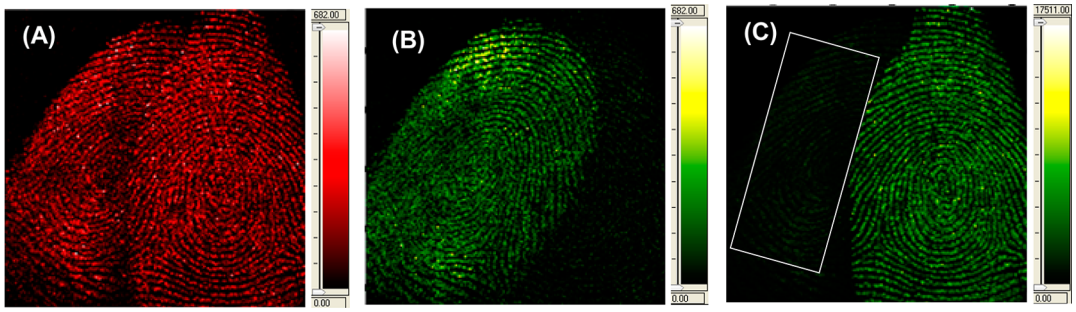

Figure 6. (A) LAET MS imaging of two overlapped latent fingerprints at m/z 311. (B) Resolved imaging at m/z 164.0427 for an unknown molecule. (C) Resolved imaging at m/z 265.1240 for dienestrol hormone.

The ability of LAET MS to detect gender related hormones actually provides a rapid means to detect these prohibited chemicals in cosmetic skin care products such as facial creams, body lotions, and moisturizers. These substances have been banned by both the European Union Directive 76/768/EEC and Hygienic Standard for Cosmetics of China because of the health risks. Currently, analysis of hormones abuses present in cosmetic skin care often includes several wet chemical steps such as sample preparation, chromatographic separation, and mass spectrometric identification.[33] LAET MS imaging offers improved throughput and sensitivity without any sample preparation.

Deconvolution of Overlapped Latent Fingerprints. A distinguished ability of LAET MS imaging is to resolve overlapped latent fingerprints based on chemical differences. Experimental procedures are the same as that of single fingerprint analysis. Different ions were extracted from full scan LAET MS experiments. Figure 6 (A) shows two very faint overlapped latent fingerprints at m/z 311 which is the negative ion of long chain fatty acid C20:0. Because fatty acids are often present in human sweat, their presence is not unique for individual identity. The key to resolve overlapped latent fingerprints is to discover characteristic ions resulting from individual life styles and occupational habits as well as biomarkers of individual metabolites. Figure 6 (B) is the LAET MS imaging of an ion extracted at m/z 164.0427 of an unknown molecule that has higher abundance in the left person's fingerprint. Figure 6 (C) is the LAET MS imaging of an estrogen dienestrol extracted at m/z 265.1240 (error: 0.0011 Da). It was shown that the right person has a much higher level of dienestrol than that of the left person, although the white square indicates the presence of this metabolite in the left person too. Please note the absolute intensity of the ion at m/z 265.1240 shown in Figure 5 (A) which was collected from the same female volunteer on a different day is 20272, and the absolute intensity of the same ion shown in Figure 6 (C) is 17511. It reveals that the level of hormones varies not only among different individuals but also varies among different days for the same individual.

CONCLUSIONS AND PERSPECTIVES

All experimental results demonstrate the potential capability of the LAET MS approach for imaging analysis of latent fingerprints, not only the physical shape containing all level features but also molecular specificities. In this approach, chemicals are identified by accurate m/z ratios and confirmed by simultaneously generated fragment ions through unpaired-electron initiated α bond cleavages without MS/MS processes. Because *in situ* generated tunneling electrons with low kinetic energies (20 eV) are exothermally captured by charge-deficient atoms, there is no redistribution of vibrational energies and nonspecific bond cleavages can be avoided. Therefore, resultant fragment ions should contain more structural specificities for accurate identification of unknown chemicals. Spatial resolution of the LAET MS technique is determined by the laser beam size, scanning step size, and actual areas the analytes desorbed and ionized as well as other factors. Particularly, compressed thin films of semiconductor materials under high pressure eliminate uneven distribution of matrix materials confronted in regular MALDI imaging, which provide LAET MS not only improved quantitative capability but also enhanced spatial resolution. Finally, because semiconductor materials do not evaporate and generate peaks in the low mass region, there is no interferences for analysis of small molecules and no contaminations for the ion source chamber of the mass spectrometer.

The unique feature of the LAET MS technique is the point electron emitting. With laser irradiation, these electrons with enough kinetic energies resonantly escape away from the surface of semiconductor materials and are accelerated in the external static electric field, eventually captured by adsorbed organic molecules. It provides a new type of ionization and fragmentation technique. One disadvantage of LAET compared with DESI is the limited ability for imaging in crime scenes. Research efforts are currently focused on the development of new techniques that can efficiently transfer latent fingerprints left on different surfaces to the thin film. Preliminary experiments have demonstrated that direct transfer of latent fingerprints from glass surfaces to the thin film by hard impression is possible although the quality is still poor at this time as shown in Supplementary Figure 4.

ASSOCIATED CONTENT

Supporting Information

Supplementary Figures 1−4. This material is available free of charge via the Internet at http://pubs.acs.org

AUTHOR INFORMATION

Corresponding Author

*E-mail: hyzhong@mail.ccnu.edu.cn.

Author Contributions

Xuemei Tang and Lulu Huang contributed equally to this work. They performed all experiments and repeated with each other. Wenyang Zhang has been involved in the use of the software of ChemDraw of all molecular structures. Hongying Zhong developed the concept, designed all experiments, analyzed all data, and wrote the manuscript.

DOI: 10.1021/ac504693v
Anal. Chem. 2015, 87, 2693−2701

Notes

The authors declare no competing financial interest.

■ ACKNOWLEDGMENTS

We greatly appreciate the support from the National Natural Science Foundation of China (NSFC, 21175054, 31270876, 31370815), Program for Changjiang Scholars and Innovative Research Team in University (PCSIRT, no. IRT0953), Hubei Natural Science Foundation Council (HBNSFC, 2009CDA001), Research Funds of Central China Normal University from the Ministry of Education (120002040270, CCNU11G01007, CCNU11C01002), and the Research Platform of Hubei Province for Monitoring of Pesticide Residues and Agricultural Products Safety.

■ REFERENCES

(1) Lewontin, R. C.; Hartl, D. L. *Science* **1991**, *254*, 1745−1750.
(2) Tate, C. M.; Nuriez, A. N.; Goldstein, C. A.; Gomes, I.; Robertson, J. M.; Kavlick, M. F.; Budowie, B. *Forensic Sci. Int.: Genet.* **2012**, *6*, 185−190.
(3) Tang, H. W.; Lu, W.; Che, Z. M.; Ng, K. M. *Anal. Chem.* **2010**, *82*, 1589−1593.
(4) Xu, C.; Zhou, R.; He, W.; Wu, L.; Wu, P.; Hou, X. *Anal. Chem.* **2014**, *86*, 3279−3283.
(5) Jain, A. K.; Chen, Y.; Demirkus, M. *IEEE Trans. Pattern Analysis Machine Intelligence* **2007**, *29*, 15−27.
(6) Hazarika, P.; Jickells, S. M.; Wolff, K.; Russell, D. A. *Angew. Chem., Int. Ed.* **2008**, *47*, 10167−10170.
(7) Drapel, V.; Becue, A.; Champod, C.; Margot, P. *Forensic Sci. Int.* **2009**, *184*, 47−53.
(8) Hazarika, P.; Russell, D. A. *Angew. Chem., Int. Ed.* **2012**, *51*, 3524−3531.
(9) Leggett, R.; Lee-Smith, E. E.; Jickells, S. M.; Russell, D. A. *Angew. Chem., Int. Ed.* **2007**, *46*, 4100.
(10) Ifa, D. R.; Manicke, N. E.; Dill, A. L.; Cooks, R. G. *Science* **2008**, *321*, 805.
(11) Croxton, R. S.; Baron, M. G.; Butler, D.; Kent, T.; Sears, V. G. *Forensic Sci. Int.* **2010**, *199*, 93−102.
(12) Akiba, N.; Saitoh, N.; Kuroki, K.; Kurosawa, K. *J. Forensic Sci.* **2011**, *56*, 754−759.
(13) Li, K.; Qin, W.; Li, F.; Zhao, X.; Jiang, B.; Wang, K.; Deng, S.; Fan, C.; Li, D. *Angew. Chem., Int. Ed.* **2013**, *52*, 11542−11545.
(14) Xu, L. R.; Li, Y.; Wu, S. Z.; Liu, X. H.; Su, B. *Angew. Chem., Int. Ed.* **2012**, *51*, 8068−8072.
(15) Ricci, C.; Bleay, S.; Kazarian, S. G. *Anal. Chem.* **2007**, *79*, 5771−5776.
(16) Song, W.; Mao, Z.; Liu, X. J.; Lu, Y.; Li, Z. S.; Zhao, B. *Nanoscale* **2012**, *4*, 2333−2338.
(17) Bright, N.; Webb, R. P.; Bleay, S. *Anal. Chem.* **2012**, *84*, 4083−4087.
(18) Bradshaw, R.; Bleay, S.; Wolstenholme, R.; Clench, M. R.; Francese, S. *Forensic Sci. Int.* **2013**, *232*, 111−124.
(19) Forbes, T. P.; Sisco, E. *Analyst* **2014**, *139*, 2982−2985.
(20) Bleay, S. *Sci. Justice* **2014**, *54*, 1−2.
(21) Wiseman, J. M.; Ifa, D. R.; Zhu, Y.; Kissinger, C. B.; Manicke, N. E.; Kissinger, P. T.; Cooks, R. G. *Proc. Natl. Acad. Sci. U. S. A.* **2008**, *105*, 18120−18125.
(22) Kertesz, V.; Van Berkel, G. J. *Rapid Commun. Mass Spectrom.* **2008**, *22*, 2639−2644.
(23) Li, B.; Hansen, S. H.; Janfelt, C. *Int. J. Mass Spectrom.* **2013**, *348*, 15−22.
(24) Wu, C.; Dill, A. L.; Eberlin, L. S.; Cooks, R. G.; Ifa, D. R. *Mass Spectrom. Rev.* **2013**, *32*, 218−243.
(25) Kertesz, V.; Van Berkel, G. J. *Rapid Commun. Mass Spectrom.* **2008**, *22*, 2639−2644.
(26) Comett, D. S.; Reyzer, M. L.; Chaurand, P.; Caprioli, R. M. *Nat. Methods* **2007**, *4*, 828−833.
(27) Casadonte, R.; Caprioli, R. M. *Nat. Protoc.* **2011**, *6*, 1659−1709.
(28) Schwamborn, K.; Caprioli, R. M. *Nat. Rev. Cancer* **2010**, *10*, 639−645.
(29) Pirman, D. A.; Reich, R. F.; Kiss, A.; Heeren, R. M. A.; Yost, R. A. *Anal. Chem.* **2013**, *85*, 1081−1089.
(30) Djidja, M. C.; Chang, J.; Hadjiprocopis, A.; Schmich, F.; Sinclair, J.; Mrsnik, M.; Schoof, E. M.; Barker, H. E.; Linding, R.; Jorgensen, C.; Erler, J. T. *J. Proteome Res.* **2014**, *13*, 2279−2313.
(31) Zhong, H.; Fu, J.; Wang, X.; Zheng, S. *Anal. Chim. Acta* **2012**, *729*, 45−53.
(32) Huang, L.; Xiao, X.; Xie, Y.; Kageruka, H.; Zhou, Y.; Deng, F.; Zhong, H. *Anal. Chim. Acta* **2013**, *786*, 85−94.
(33) Takahiro, D.; Keiji, K.; Satoshi, T.; Shuzo, T.; Shozo, I. *J. Chromatogr. B: Anal. Technol. Biomed. Life Sci.* **2009**, *877*, 1005.

DOI: 10.1021/ac504693v
Anal. Chem. 2015, 87, 2693−2701